Submitted for publication in Journal of Geophysical Research : Solid Earth

Supporting Information for

Cohesion and Initial Porosity of Granular Fault Gouges control the Breakdown Energy and the Friction Law at the Onset of Sliding

N. Casas [1,2*], G. Mollon[1], and A. Daouadji[2]

1 Univ. Lyon, INSA-Lyon, CNRS UMR5259, LaMCoS, F-69621, France.
2 Univ. Lyon, INSA-Lyon, GEOMAS, F-69621, France.]

Corresponding author: Nathalie Casas (nathalie.casas@insa-lyon.fr)

Contents of this file

Additional Supporting Information (Files uploaded separately)

Introduction

The following paragraphs present: (S1) the numerical setup and parameters used in the study for direct shear experiment, (S2) the methodology and results allowing to determine the Representative Surface Element (RSE), (S3) the method used to compute the initial porosity selected for numerical modelling (i.e. dense and mid-dense sample), (S4) how to pass from a numerical cohesion to a percentage of cohesion within the gouge, (S5) tables of main results of DEM modelling and gouge kinematics, (S6) the formula used to calculate the energy consumption during numerical experiments, (S7) detailed and validation for the proposed simplified model.

S1. Numerical setup and parameters for direct shear experiment

S1.1: 2D Numerical granular sample

Paking2D downloadable here.

Table S1. Parameters used for grain generation.

Property	Value
Distribution type	fractal
Parameter of distribution	D=2.6
Sample size	2 x 20 mm

S1.2: 2D Direct shear experiment with DEM

MELODY 2D downloadable here.

Table S2. Numerical properties for direct shear experiment.

Property	Value
Normal stress	40 MPa
Shear velocity	1 m/s
Volumetric mass	2600 Kg/m3 (grains) 26 Kg/m3 (rock walls)
Numerical stiffness	1E+15 N/m^3
Inter-particular friction	0.5
Sample size	2 x 20 mm
Number of particles	4960

Table S3. Numerical setup and solver

Property	Value
Constant time step (Euler scheme)	1e-9 s
Contact updating period	1e-7 s

S2. Representative Surface Element (RSE)

In order to justify a RSE, three different sizes of model have been studied with identical numerical parameters. The differences sizes of models (6x2mm², 10x2mm² and 20x2 mm²) induce a change in the total number of particles in order to keep the same equivalent diameter for grains (respectively 1500, 2500 and 5000 grains). By increasing the number of grains in the model as well as the length of the gouge, we observe similar behaviours of the sheared gouge layers. Friction coefficient follows the same trend for the three size of model. The friction peak μ_p is of the same order of magnitude (0.73-0.78). A small difference is observed for the case with 2500 grains, where the friction peak is more important, probably due to a slightly different stacking of the particles during the compaction of the sample (Figure S1). As the number of grains increases, there is therefore an increase in normal and tangential forces applied to the upper rock wall. The number of grains is higher, but the gouge size also increases, making possible to maintain a similar coefficient of friction in the three models. The friction curve obtained with the 1500-grains sample are noisier, because the dynamic effects are more noticeable with fewer grains. However, by comparing force chains in the gouge for the three models, we do not see significant changes (Figure S2 – a). They are oriented at 30-45 ° relatively to the upper rock wall and normal forces seem oriented in this same direction (Figure S2 –b). Using 5000 grains seems to give a sufficiently representative behaviour to observe local mechanisms. It is therefore not necessary to represent a larger model for this type of micromechanical study.

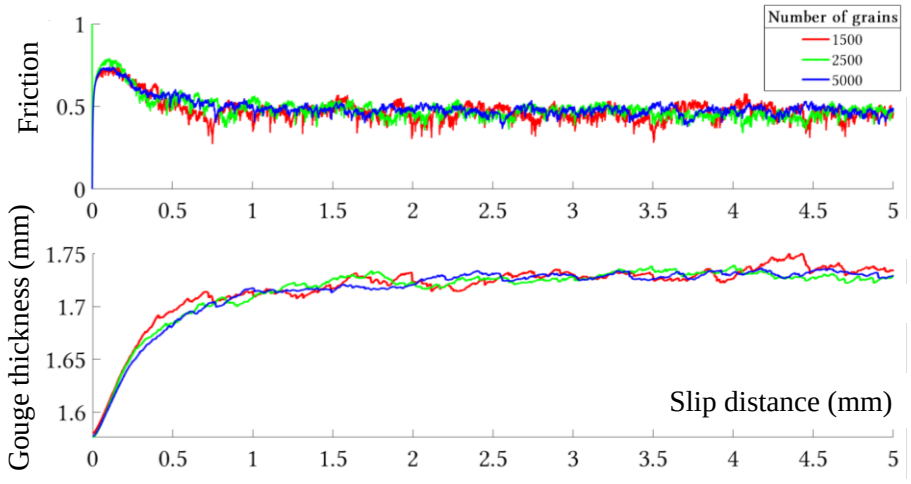

Figure S1. Friction coefficient and gouge thickness (mm) as functions of the slip distance (mm), small sample with 1500 particles in red, middle-size sample with 2500 particles in green and large sample used in the paper with 5000 grains in blue.

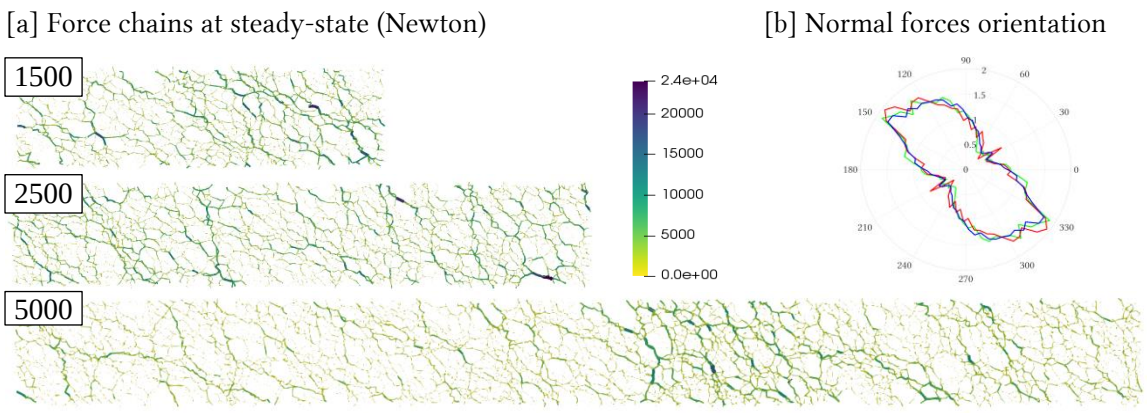

Figure S2. [a] Force chains magnitude in Newton for 1500 grains, 2500 grains and 5000 grains – [b] Number of contacts with a normal vector oriented in a given direction (using polar diagrams where the Theta-axis is the orientation and the R-axis is the number of contacts), Normal forces orientation as a function of the model, at steady state. Small sample with 1500 particles in red, the middle sample with 2500 particles in green and the sample used in the paper with 5000 grains in blue.

S3. Initial porosity and intergranular friction

To have an evolution of the initial porosity inside gouge samples, we compacted eleven samples with inter-particle friction coefficients between 0 and 1, allowing to obtain more or less dense grain stacks. With a zero inter-particle friction coefficient, the only contact parameter between grains is the numerical stiffness. The packing obtained is in a very dense state, with a solid fraction close to 0.89 (i.e. porosity of 0.11). In the opposite, adding a friction coefficient of 1 between each contact hinders movements and contacts and results in a much less dense sample (0.83). The idea is, therefore, to see the influence of this initial state on gouge shearing. The compaction of samples was carried out on a sample of 4960 grains generated according to a fractal distribution law (dimension factor D = 2.6), i.e. with the same initial sample before compaction step. Parameters used for samples compaction are written in Table S2.

Eleven samples were created and solid fraction was measured at the end of the compaction step. The solid fraction (F_S) is the ratio of the surface occupied by the grains to the apparent surface of the sample. Since we are here in 2D, we will take an area rather than a volume considering that the 3rd dimension is the same in the numerator and denominator. In the associated paper, we talk about the percentage of porosity (i.e. the ratio of the surface

occupied by voids to the apparent surface of the sample) rather than solid fraction. The solid fraction and porosity in a sample can therefore be calculated as follows, with S an area:

$$F_S = \frac{S_{grains}}{S_{gouge}} \quad (1)$$

$$S_{gouge} = S_{grains} + S_{void} \quad (2)$$

$$P_S = \frac{S_{voids}}{S_{gouge}} \quad (3)$$

Figure S3 displays the solid fraction and gouge thickness (mm) for each sample generated with a different inter-particle friction coefficient. We observe that gouge thickness decreases with the increase of solid fraction. The highest solid faction (0.89) corresponds to a very dense sample in which there is very few porosity between grains. In contrast, the lowest solid fraction (0.83) corresponds to a slightly less dense sample, with a gouge thickness of 0.12 mm greater, (5% of the total thickness). We can see the representation of this solid fraction in Figure S4. Samples used in the associated paper are sample 10 (F_S=0.89 or Ps=11%) and 15 (F_S=0.84 or Ps=16%).

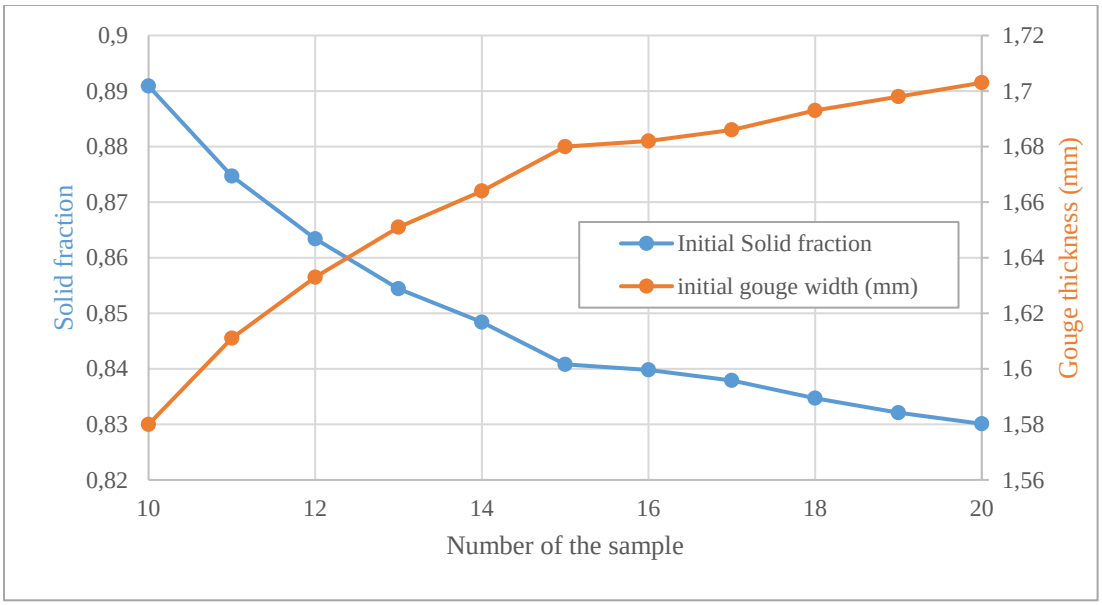

Figure S3. Evolution of solid fraction (in blue) and gouge thickness (in orange) as a function of the inter-particle friction used to compact samples (replaced by a sample number). The sample 10 corresponds to a zero friction and the 20 to a friction equal to one.

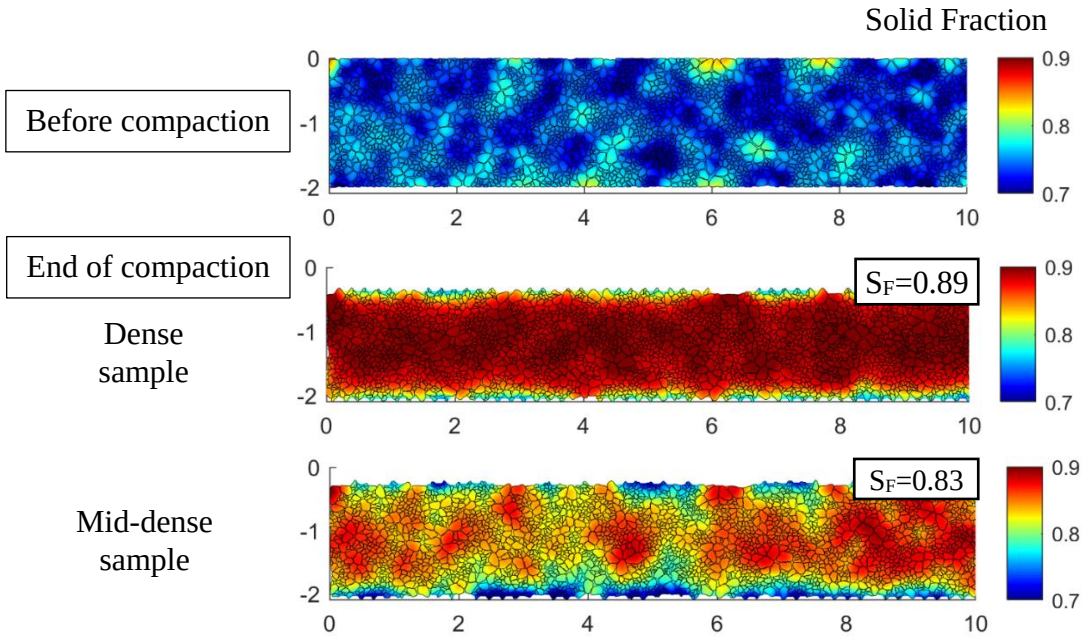

Figure S4. Solid fraction at different step of the simulation – half of a fault segment (0 -10mm). The first line displays the initial solid fraction before compaction (solid fraction between 0.7 and 0.8). At the end of compaction, we can clearly distinguish the difference between a very dense sample, with a homogeneous and high solid fraction over the entire gouge (i.e. lower porosity of 11%) and a mid-dense sample with an less homogeneous solid fraction (i.e. higher porosity of 17%), which depends on the stacks of grains created during the compaction.

S4. Percentage of cohesion within the gouge

To quantify the total amount of cohesion energy in the initial state of the fault (i.e. the energy that would be needed in order to break all the initial bonds), we normalize it with respect to a representative energy. This quantity corresponds to a surface energy of 62J/m² (reported for the Chilhowee quartzite and considered as an upper limit for rock surface energy in (Friedman et al., 1972)) applied on the whole external surface of all the grains present in the simulation (a unit length is considered in the third dimension for any necessary purpose). This would correspond to 100% of cohesion, and we explore the influence of this percentage in the paper (Figure 3 – c). Detailed calculi are explained in this Section.

The maximal energy for a fault patch of 1m² and for cemented bonds covering the total external surface of all particles in the gouge can be written as:

$$E_{max} = 2U\frac{P_{tot}}{L_{gouge}} \tag{4}$$

With U = 62J/m², P_{tot} the sum of the perimeter of all grains in [m] and L_{gouge} the length of the fault model in [m]. In our model, the energy to break all cohesive bonds on a 1m² fault patch can be defined as $E_C\ (J/m^2)$, the energy of de-cohesion, representing the energy needed by the system to break all cohesive bonds initially present in the gouge. It can be described by a relation between properties of the initial contact network (cumulated length of all the contacts $L_{intact-tot}$ and number n of contacts, stiffness k), and the initial numerical cohesion C_{num} for each contact and the length L_{gouge} of the model:

$$E_C = L_{intact-tot}\left(\frac{C_{num}}{2}\right)^2\frac{1}{2\,k\,L_{gouge}} \tag{5}$$

Supposing that the maximum apparent surface energy needed by the gouge to break a bond is E_{max}, for a fully cemented material. We determine the value $C_{num-100\%}$ of numerical cohesion, which corresponds to a cohesion of 100% based on the definition given above. We can thus express the cohesive energy in our initial sample as a percentage of cohesion $X\%$ in comparison to the 100% cohesion.

$$E_C = E_{max} \tag{6}$$

$$C_{num-100\%} = \sqrt{\frac{16\, E_{max}\, P_{tot}\, k}{L_{intact-tot}}} \tag{7}$$

$$X\% = \left(\frac{C_{num}}{C_{num-100\%}}\right).100 \tag{8}$$

S5. Results and Gouge kinematics

Results obtained with numerical setup and properties displayed in Table S2:

Table S4. Results for dense samples (initial porosity of 11% or solid fraction SF=0.89). With Δτ (Pa) the stress drop from the friction peak to the plateau, μ_{SS} the steady-state friction, μ_p the friction peak, SF_{SS} the steady state solid fraction, P_{SS} the steady-state porosity, Ep_{SS} the steady-state gouge thickness.

C_{num}	100	200	500	800	1000	1200	1500	2000	2500
% cohesion	4	8	19	30	38	46	57	76	95
Δτ (Pa)	1.08+07	1.11E+07	1.82E+07	3.01E+07	3.66E+07	4.20E+07	5.27E+07	6.84E+07	8.75E+07
μ_{SS}	0.481	0.482	0.490	0.477	0.496	0.484	0.475	0.473	0.431
μ_p	0.771	0.786	0.994	1.406	1.695	1.938	2.376	3.094	3.838
SF_{SS}	0.869	0.867	0.876	0.877	0.869	0.87	0.884	0.895	0.889
P_{SS}	0.131	0.133	0.124	0.123	0.131	0.13	0.116	0.105	0.111
Ep_{SS} (mm)	1.72	1.726	1.707	1.705	1.72	1.719	1.691	1.671	1.681

The representation of the relative damage gives a picture of the state of decohesion between grains and its location within the gouge. This damage is set to 0 when cohesive bonds are first established (all the bonds are intact) and may evolve until 1 if all these bonds reach the "broken" status (cf. Section 2.3 in the associated paper). It is thus a relative damage with respect to an initial state. The following movies illustrate the evolution of the gouge state as a function of the slip distance:

Movie S1. Comparison of the evolution of relative damage with slip distance for dense samples (entire granular gouge), between 8% cohesion (mildly cohesive regime) and 38% cohesion (cohesive regime). From zero imposed slip [A] to the beginning of steady state [G].

Movie S2. Comparison of the evolution of relative damage with slip distance for dense samples (entire granular gouge), between 38% cohesion (cohesive regime) and 95% cohesion (ultra-cohesive regime). From zero imposed slip [A] to the beginning of steady state [G].

The following movies present the evolution of solid fraction as a function of the slip distance for the three regimes highlighted in the paper. Another way to observe Riedel bands and cracks within the gouge.

Movie S3. Solid fraction in dense sample (entire granular gouge) as a function of the slip distance for 8% cohesion (mildly cohesive regime). From zero imposed slip [A] to the beginning of steady state [G].

Movie S4. Solid fraction in dense sample (entire granular gouge) as a function of the slip distance for 38% cohesion (cohesive regime). From zero imposed slip [A] to the beginning of steady state [G].

Movie S5. Solid fraction in dense sample (entire granular gouge) as a function of the slip distance for 95% cohesion (ultra-cohesive regime). From zero imposed slip [A] to the beginning of steady state [G].

Table S5. Results for mid-dense samples (initial porosity of 16% initial solid fraction SF=0.84) With $\Delta\tau$ (Pa) the stress drop from the friction peak to the plateau, μ_{SS} the steady-state friction, μ_p the friction peak, SF_{SS} the steady state solid fraction, P_{SS} the steady-state porosity, Ep_{SS} the steady-state gouge thickness.

C_{num}	*100*	*200*	*500*	*800*	*1000*	*1200*	*1500*	*2000*
% $cohesion$	3	6	18	31	40	50	66	95
$\Delta\tau$ *(Pa)*	3.02E+06	2.60E+06	3.69E+06	9.06E+06	1.39E+07	1.92E+07	2.61E+07	3.57E+07
μ_{SS}	0.461	0.466	0.460	0.458	0.469	0.479	0.476	0.455
μ_p	0.536	0.531	0.552	0.684	0.815	0.959	1.130	1.346
SF_{SS}	0.855	0.854	0.852	0.85	0.851	0.857	0.864	0.858
P_{SS}	0.145	0.146	0.148	0.15	0.149	0.143	0.136	0.142
Ep_{SS} *(mm)*	1.749	1.752	1.756	1.766	1.757	1.745	1.73	1.742

S6. Energy Budget

The following section presents the energy budget of the model divided into three contributions theoretically described as dilatancy, friction and decohesion (Section 3.3 and 4.1 in the associated paper). Each formula corresponds to one different mechanism. (Figure S5 – a) displays the evolution of energy consumption as a function of the slip distance for all contributions for a dense case with 57% of cohesion. We can also observe the associated friction (Figure S5 – b) used to create simplified models in Section 3.3. (Figure S5 – c & d) helps analysing the percentage of energy consumed in pre-peak phase and the percentage of cohesion remaining in the sample with the increasing slip distance. The total energy is calculated at every time step with the formula bellow.

$$E_{tot}(t) = E_{tot}(t-1) + \frac{[D_x(t) - D_x(t-1)] * [F_x(t) + F_x(t-1)]}{2 * S_{gouge}} \quad (9)$$

With t the current time step, D_x the horizontal displacement of the upper rock wall, F_x the tangential forces acting on the upper rock wall and $S_{gouge} = L_{gouge} * 1$ (2D).

The Dilatancy energy is, at every time step:

$$E_{dilatancy}(t) = \frac{[D_y(t)] * [F_y(t)]}{S_{gouge}} \quad (10)$$

With D_y the vertical displacement of the upper rock wall, F_y the normal forces acting on the upper rock wall.

It is also possible to calculate an averaged post-peak Dilatancy energy :

$$E_{mid-dil} = \left[D_{y_{ss}} - H_{peak}\right] * \sigma_N \quad (11)$$

With $D_{y_{SS}}$ the gouge thickness at steady-state, H_{peak} the gouge thickness at friction peak and σ_N the normal stress.

The Decohesion energy at every time step is: (12)

$$E_{damage}(t) = L_{contact} * \left[\frac{C_{num}}{2}\right]^2 * \frac{1}{2k_n} * \frac{1}{S_{gouge}}$$

With $L_{contact}$ the total length of contacting grains, C_{num} the numerical cohesion described in S4 and k_n the numerical stiffness.

Friction and elastic energies at every time step results in the remaining energy of the model:

$$E_{friction}(t) = E_{tot}(t) - E_{dilatancy}(t) - E_{damage}(t) \quad (13)$$

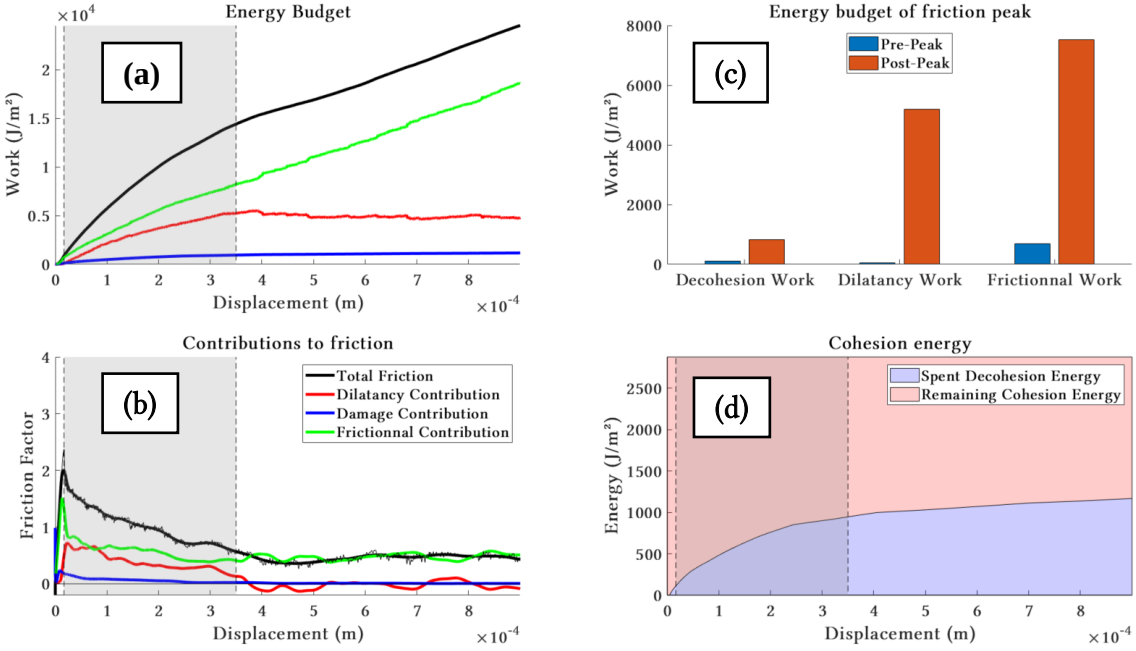

Figure S5. Dense sample with 57% of cohesion (a) Energy budget as a function of slip displacement for the different contributions, (b) Friction coefficient extracted from energy consumption, (c) Energy budget in pre-peak or post-peak phase, (d) Cohesion spent and remaining in the sample as a function of the slip distance.

S7. Simplified model – validation

The Figure S7 (present in the paper) displays the proposed evolution for each parameter used in the simplified models, as a function of the cohesion after fitting on all the simulation data.

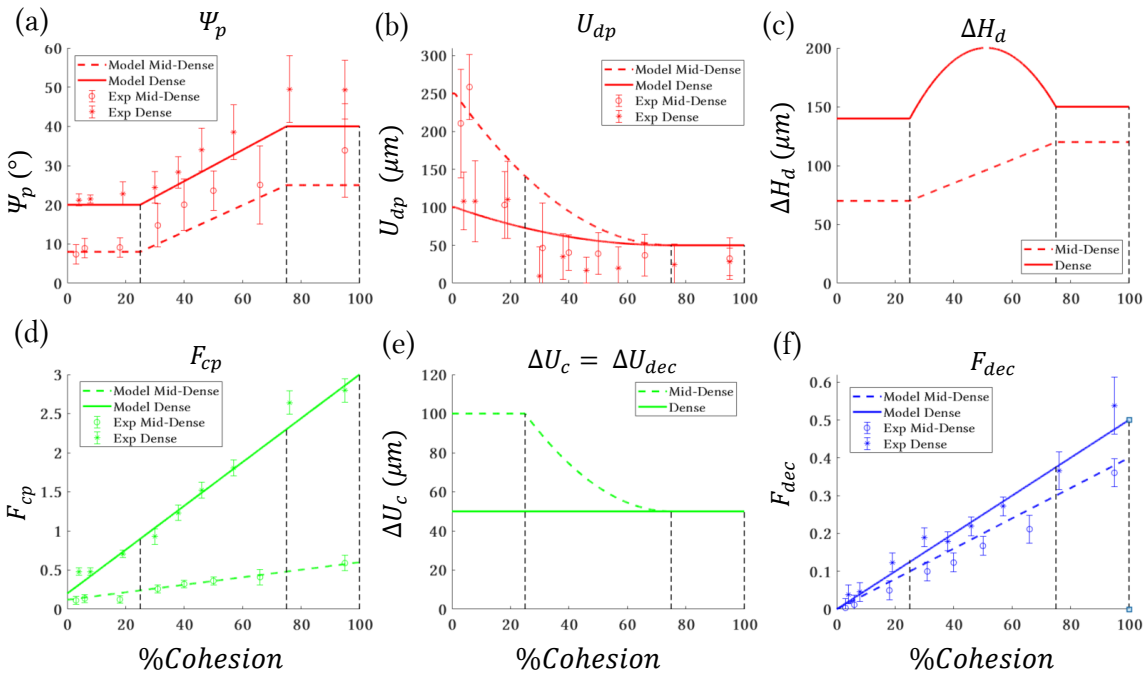

Figure S6. Model of friction laws presenting the 7 parameters taken into account in the simplified models. It can be noted that k, μ_{SS}, and ΔU_{cpp} do not depend on cohesion. (a) Maximum dilatancy angle Ψp. (b) Slip distance corresponding to the maximum dilatancy U_{dp}. (c) Gain in gouge thickness at the end of the dilatancy phase ΔH_d. (d) Peak friction at the end of the elastic phase F_{cp} and post peak friction F_{cpp} . (e) Characteristic distance of the exponential decay ΔU_c. (f) Maximum friction induced by decohesion F_{dec}. Dots are experimental data derived from DEM modelling. They may be not aligned with numerical modelling as some peak values are difficult to identify on raw data and the error can be important. ΔH_d and ΔU_c do not have experimental data, as they are completely created for the model.

Dilatancy parameters are not following linear laws and both mildly and ultra-cohesive regimes present constant values, meaning that the major evolution occurs in the transitional cohesive regime [Figure S6 – a, b, c]. As Ψ_p is increasing with the percentage of cohesion. the slip distance associated to this maximum is reducing. The more cohesion is added, the earlier the maximum dilatancy is observed. These results are consistent with the associated paper related to the main behaviour of the gouge regarding the initiation of sliding. ΔH_d

gives the shape of the Gaussian model. Even though a lognormal law seemed to better fit the dilatancy friction curves than a Gaussian law, it was not satisfactory for global friction models. The objective of this simplified model is not to reproduce the exact location of dilatancy friction peak, but to model a global and consistent shape evolution from one case to another.

Pushing up cohesion increases Coulomb friction peak and post peak friction that follow a linear law (Figure S6 – d). The fact that denser samples have a superior friction peak may be due to the higher number of contacts of each particle that generates more resistance to sliding. The characteristic distance ΔU_c remains almost constant for dense samples, but decreases for mid-dense samples as a function of the cohesion (Figure S6 – e). This evolution is related to the type of Coulomb model observed: a larger distance of decay for asymptotic models (Figure 13 – d in the paper).

For decohesion contribution, F_{dec} evolves as a rising linear law from 0 to 100% cohesion [Figure S6 – f] in accordance with previous results (Section 3.3 in the paper).

It can be noted that ΔU_{cpp}, k and μ_{SS} are independent of cohesion and taken as constant. The slip distance ΔU_{cpp} is equal to 8 µm for dense samples and 40 µm for mid-dense samples. The gouge layer stiffness k is found to be equal to 140 kN/m for dense samples and to 80 kN/m for mid-dense samples.

The Figure S7 below presents the simplified models and the initial curves values. The total friction is the black curve, sum of the contributions of: the dilatancy friction (red), the Coulomb friction (green) and of the decohesion friction (blue). These contributions are calculated thanks to global potential energy recovered at each time step, from the data set presented in previous sections and computations details presented in S1. The detailed model is presented in Section 2 in the paper. Six chosen cases are presented here to validate the experimental friction curves with the friction decomposition proposed: one case for each regime described in Section 3.2 (mildly cohesive, cohesive and ultra-cohesive) and for each type of compacted sample (dense and mid-dense).

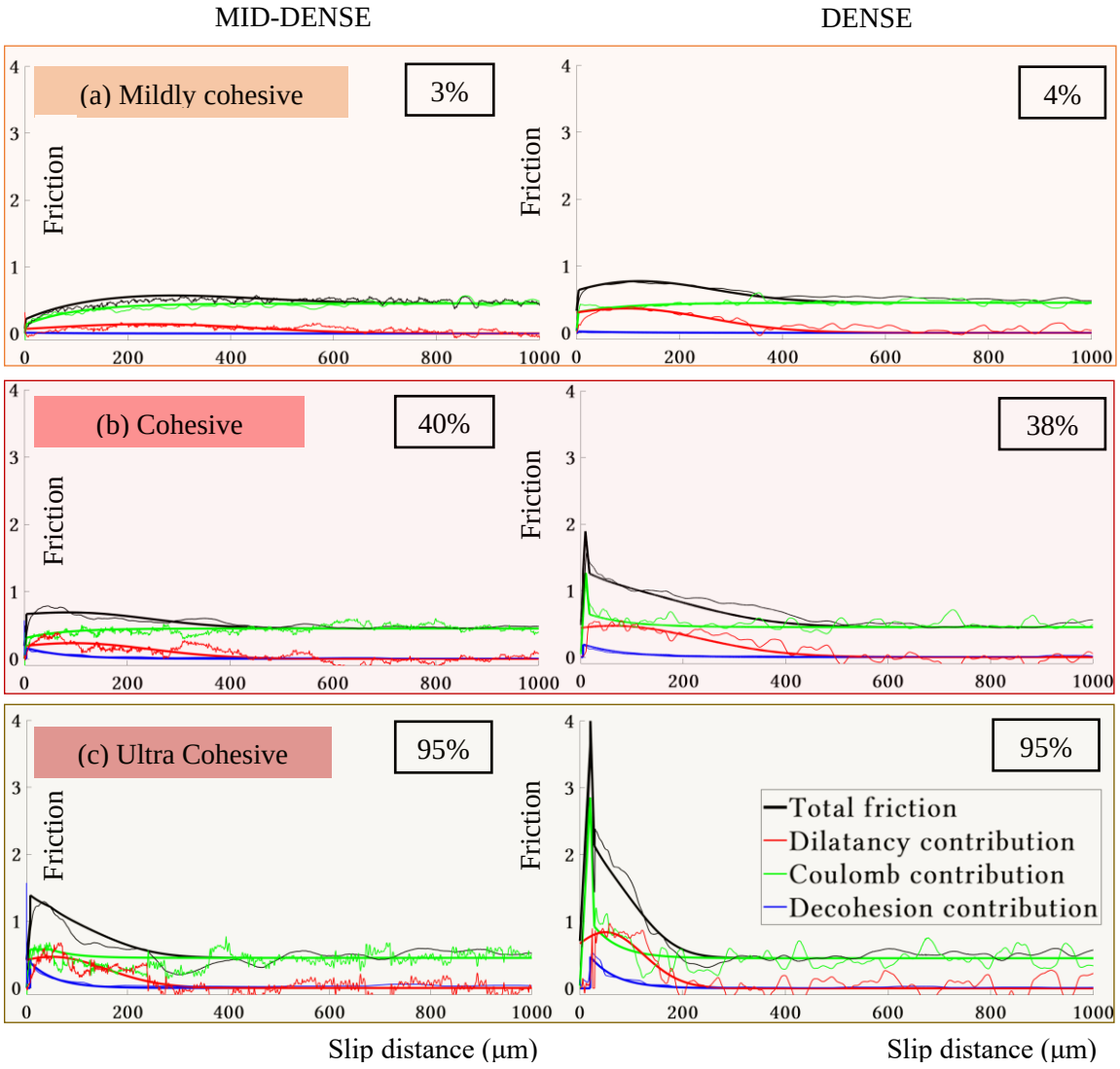

Figure S7. Mid-dense and dense models – validation as a function of the percentage of cohesion. Friction-slip curve with different contributions (dilatancy in red, Coulomb in green and decohesion in blue), the black curve is the sum of all contributions. (a) mildly cohesive regimes, where the observed pre-peak phase is important - (b) Cohesive regimes with a diminution of the pre-peak phase with the increase of cohesion - (c) Ultra cohesive regimes with almost no pre-pic phase.